Oblique-Angle Deposition of SiO_2 Alignment Layers

Monte Carlo growth model, column tilt, surface structure and predicted LC pretilt

D.F.Hakala

October 31, 2026

Table of Contents

1. Summary 1
2. Program and files 2
3. Growth model 3
4. Film structure and column tilt 4
5. Effect of surface diffusion 8
6. Liquid-crystal pretilt 9
7. Implications for the LCoS process 11
8. Calibration and measurement 12
9. Limitations 12
References 13

1. Summary

This note documents `oad_sio2_montecarlo.py` in `C:\LCoS\LCoS_Simulations\oblique_angle_deposition_Sio2_alignment_layer` and its output. The program grows an obliquely deposited (glancing-angle, GLAD) SiO_2 film on the aluminum pixel mirror one vapor particle at a time, measures the column tilt and surface structure that emerge from shadowing, and then solves for the liquid-crystal (LC) director above the simulated surface to predict the pretilt of a vertically aligned (VA) cell, dry and at two humidities. It is the link between the e-beam source model (vapor arriving at about 82° in the SpatiaLight carousel) and the VAN cell model (which takes the pretilt as an input). The LAMMPS work in the same folder is not covered here.

Main results, from three runs (pure ballistic growth; surface diffusion with E_a = 0.8 eV and 0.6 eV at 300 K), five seeds per angle unless noted:

- **Column tilt.** The simulated tilt rises from about 17–21° at α = 50° to 56–59° at 80° and 65–66° at 85°. It lies below both the tangent and Tait rules up to about 75°, crosses the Tait rule near 80°, and lies between the two at 85°.

- **Porosity.** Ballistic growth gives packing fractions from 0.17 ($\alpha = 50°$) down to 0.06 (85°). Strong diffusion ($E_a = 0.6$ eV) roughly doubles the density at every angle (0.41 to 0.09) but flattens the tilt at glancing angles ($\beta \approx 49°$ at 85°).
- **Weak diffusion changes nothing.** With $E_a = 0.8$ eV each surface atom hops about 0.36 times per monolayer, and the results match pure ballistic growth within the seed-to-seed scatter. This run also reproduces the October 16 run in the folder exactly.
- **Surface.** RMS roughness is about 3–5 nm up to $\alpha = 75°$, then 8 nm at 80° and 17 nm at 85°, with ridges about 60 nm apart at 75–80° and about 160 nm at 85° (all broad rather than strictly periodic).
- **LC pretilt (MLC-6608, homeotropic anchoring, $W = 3 \times 10^{-4}$ J/m², 4 nm smoothing).** Below $\alpha \approx 70°$ the pretilt is under 0.5° from the normal. It grows rapidly at glancing angles: −0.7° at 75°, −4.2° at 80° and −11.1° at 85° (dry), where the minus sign means tilted away from the vapor source.
- **Humidity.** Water condensing in surface valleys and weakening the anchoring increases the pretilt magnitude: at 80° it goes from 4.2° (dry) to 5.5° (50 % RH) and 6.8° (90 % RH).
- **SpatiaLight carousel.** With vapor arriving at 81.0–83.2° across a wafer, the model predicts a dry pretilt of roughly 5–9° from the normal that changes by about 3° (and more in humid conditions) from the bottom to the top of the wafer. That is consistent with the 8° assumed in the VAN cell model, but the absolute values depend on two calibration parameters (anchoring strength and smoothing length) that must be fixed against one measured pretilt.

2. Program and files

Item	Description
`oad_sio2_montecarlo.py`	Python port of `OAD_SiO2_MonteCarlo_Simulation_8_xcorr_tilt.wl`: 2D ballistic aggregation with optional thermally activated diffusion; column-tilt extraction by cross-correlation; ridge geometry; LC director-field pretilt solve with humidity. Needs numpy, scipy, matplotlib and (strongly recommended) numba
`oad_compare_runs.py` (new, with this note)	Overlays tilt, packing and pretilt from several run folders (Figure 6)
`glad_mc_output/run_<date>_<settings>/`	One folder per run: results, pretilt, ridge and profile CSV files and nine PNG figures
Reference PDFs	Lesker SiO_2 evaporation notes; BYU senior thesis on SiO_2 film characterization (LPCVD); S. Oh, nucleation and growth lecture notes; Tkachenko, Marino and Abbate (2010), spectroscopic ellipsometry of nematic LCs (pretilt and anchoring measurement); and two background papers

Commands used for this note (each took about 3 minutes with numba):

```
python oad_sio2_montecarlo.py --T 300 --Ea 0.8 --profile-angles 60 70 80 --
outdir run_Ea08
python oad_sio2_montecarlo.py --no-diffusion --profile-angles 60 70 80 --
outdir run_ball
python oad_sio2_montecarlo.py --T 300 --Ea 0.6 --seeds 3 --profile-angles 60
70 80 --outdir run_Ea06
python oad_compare_runs.py run_ball:"ballistic" run_Ea08:"Ea 0.8 eV"
run_Ea06:"Ea 0.6 eV"
```

The script's built-in defaults are E_a = 0.6 eV, five seeds and α = 50–85° in 5° steps. Two help strings are out of date: `--Ea` says the default is 1.0 eV (it is 0.6) and `--hop-cap` says 2000 (it is 4000).

3. Growth model

Lattice. Growth is simulated on a square 2D lattice in the plane of incidence. One cell is the cube root of the volume per SiO_2 unit in amorphous silica (ρ = 2.20 g/cm^3), 0.357 nm, so the 250-row lattice allows films up to 89 nm thick. The lattice width scales as 1.6 × 250 × tan α (477 cells at 50° to 4573 at 85°) so that a particle's lateral drift never wraps the periodic domain, and 12 particles are fired per unit of lattice width.

Ballistic flight. Each particle starts at a random x above the lattice and travels toward the substrate at angle α from the normal in steps of half a cell along its ray, sticking at the first site next to existing material (eight-neighbor contact). The half-cell step is the version-8 fix: earlier versions jumped tan α cells sideways per step and could tunnel through columns at glancing angles.

Surface diffusion. An atom with nothing in the three cells above it is "open" and hops at the Arrhenius rate

$$r = \nu_0 \exp\left(-\frac{E_a}{k_B T}\right) \tag{3.1}$$

with $\nu_0 = 10^{13}$ s^{-1}. Time advances by τ/n_x per arriving particle, where τ = 1 s is the time to deposit one monolayer, so between arrivals the number of hop events is Poisson-distributed with mean M r τ/n_x for M open atoms. A hop moves one random open atom to an empty neighboring site that still touches the film. Atoms buried by a new arrival stop hopping, and start again if the atom above them hops away. Only the product $\nu_0\tau$ matters, so a factor of ten in either is equivalent to shifting E_a by $k_B T \ln 10 \approx 0.06$ eV at 300 K. At 300 K, E_a = 0.8 eV gives r τ = 0.36 hops per open atom per monolayer and E_a = 0.6 eV gives 833.

Column tilt. The tilt β is measured from the film itself, not assumed. For each lag L between rows, the circular cross-correlation of row z with row z + L peaks at a lateral shift

$$s(L) = L \tan\beta \tag{3.2}$$

and β is the arctangent of the slope of s against L (lags 1–8, rows above the first 12 and below the 15 nearest the lattice top). Two analytic rules are plotted for comparison, the tangent rule of Nieuwenhuizen and Haanstra and the rule of Tait, Smy and Brett:

$$\tan\beta = 1/2 \tan\alpha \tag{3.3}$$

$$\beta = \alpha - \arcsin\left(\frac{1-\cos\alpha}{2}\right) \tag{3.4}$$

A third “Schiller-type” curve, tan β = 0.3 tan α, is drawn as a labeled placeholder; it is not a verified literature formula.

4. Film structure and column tilt

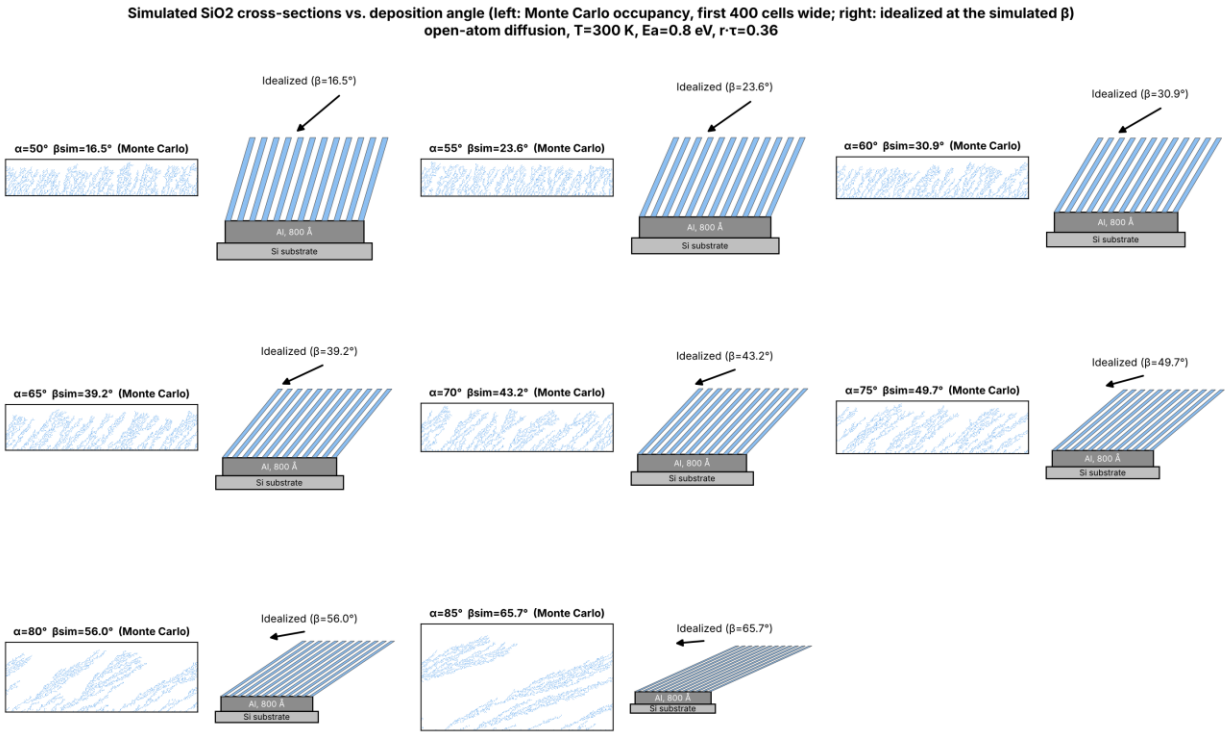


Figure 1. Simulated cross-sections (first 400 cells wide) and idealized columns at the simulated tilt for α = 50–85°, E_a = 0.8 eV at 300 K.

α (°)	Tangent rule β (°)	Tait rule β (°)	Simulated β (°)	Packing fraction	Thickness (nm)	RMS roughness (nm)	Ridge spacing (nm)
50	30.8	39.7	16.5 ± 9.0	0.168	27	4.3	19
55	35.5	42.7	23.6 ± 3.5	0.162	29	3.4	20
60	40.9	45.5	30.9 ± 5.3	0.151	30	4.0	16
65	47.0	48.2	39.2 ± 3.5	0.144	32	4.0	34
70	53.9	50.8	43.2 ± 2.2	0.128	35	4.6	24
75	61.8	53.2	49.7 ± 1.2	0.111	40	4.8	59
80	70.6	55.6	56.0 ± 0.9	0.086	52	7.9	62
85	80.1	57.8	65.7 ± 0.3	0.056	77	16.6	163

Table 4.1. Results for E_a = 0.8 eV, 300 K, five seeds (mean ± standard deviation of β). Thickness is the tallest occupied row of the first seed; ridge spacings are the dominant Fourier component of the top surface and are broad except at 50°.

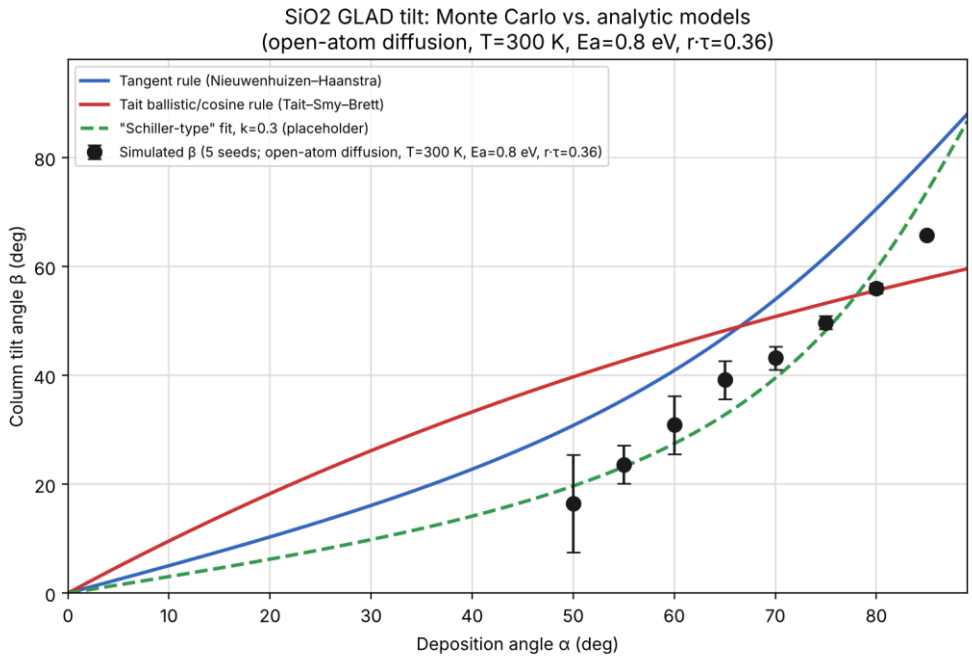


Figure 2. Simulated column tilt against deposition angle, with the tangent and Tait rules and the placeholder curve.

The simulated tilt is well defined above about 60° (scatter of a few degrees falling to 0.3° at 85°) and noisy at 50°, where the columns are short and poorly separated. At low angles the film is closer to a random porous deposit than to distinct columns, so the tilt falls below both analytic rules. At 80° the simulation agrees with the Tait rule; at 85° it is 8° above Tait and 14° below the tangent rule. Figure 3 shows that, above 60°, the tilt settles within about 40 lattice rows above the 12-row nucleation zone (roughly the first 20 nm of film) and then stays constant, so a 20–50 nm alignment layer already has its final tilt at the angles of interest.

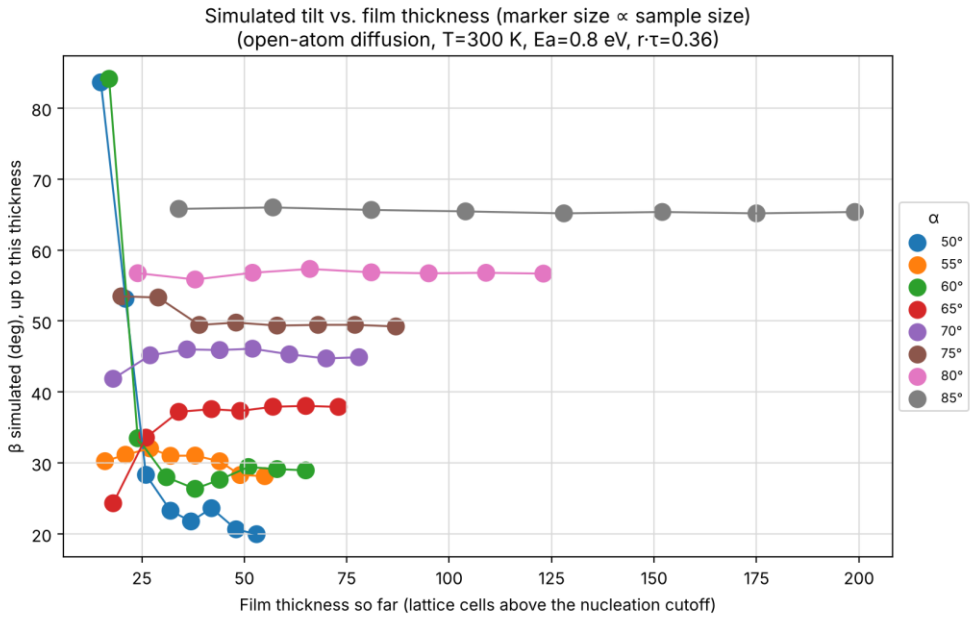


Figure 3. Simulated tilt against film thickness for each angle (marker size proportional to the number of occupied cells used).

The top surface (Figures 4 and 5) shows the sawtooth expected from shadowing: long gentle slopes facing the source and steep drops on the shadowed side. Roughness and ridge spacing both grow sharply above 75°, because the shadow length scales as tan α.

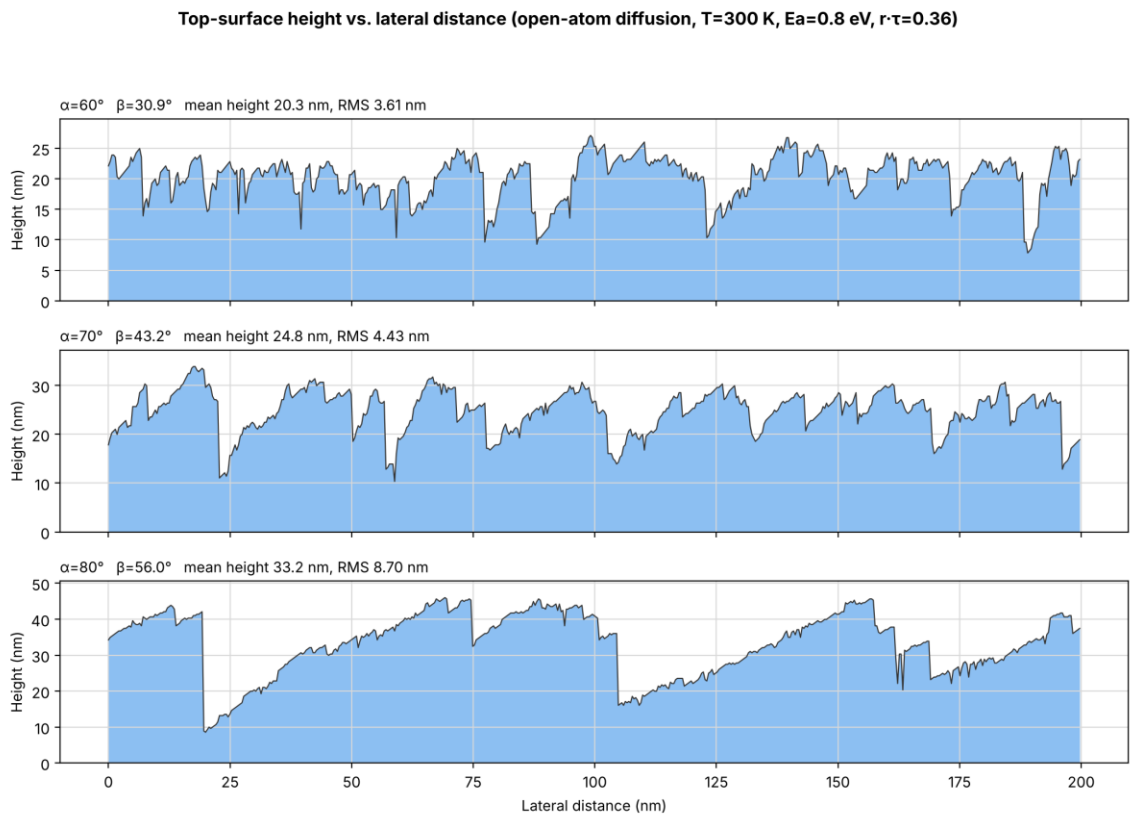


Figure 4. Top-surface height over 200 nm of film at α = 60°, 70° and 80°.

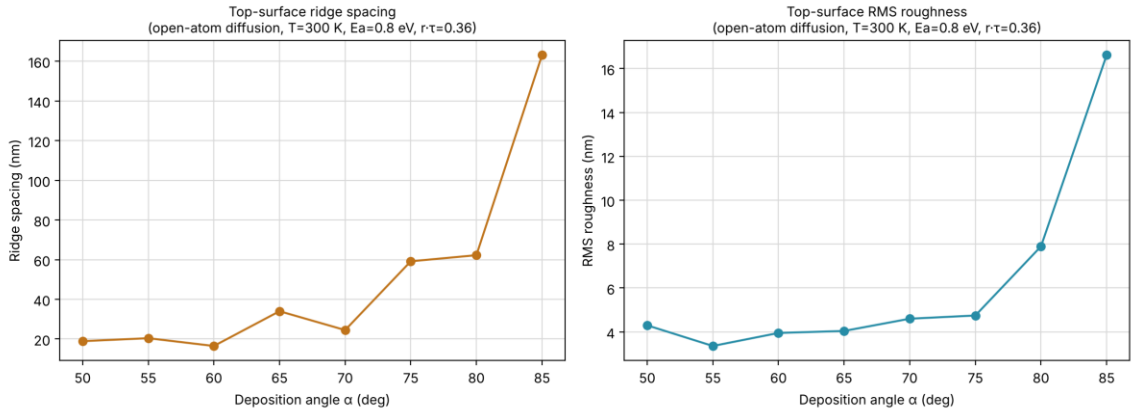


Figure 5. Ridge spacing and RMS roughness of the top surface against deposition angle.

5. Effect of surface diffusion

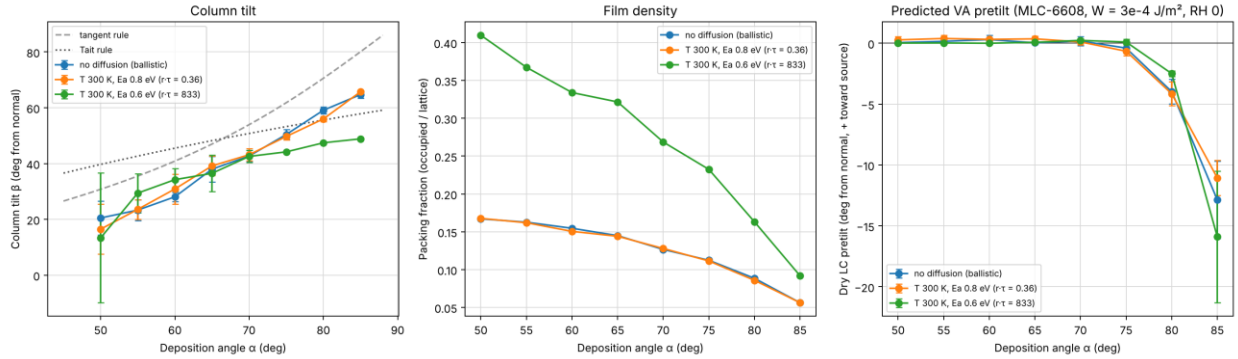


Figure 6. Comparison of the three runs: column tilt, packing fraction and dry LC pretilt against deposition angle (oad_compare_runs.py).

α (°)	β, ballistic (°)	β, E_a 0.8 eV (°)	β, E_a 0.6 eV (°)	Packing, ballistic	Packing, 0.6 eV	Pretilt dry, ballistic (°)	Pretilt dry, 0.6 eV (°)
50	20.5	16.5	13.4	0.167	0.410	+0.05	+0.01
60	28.1	30.9	34.2	0.155	0.334	+0.30	0.00
70	42.7	43.2	42.6	0.127	0.269	+0.19	+0.23
75	50.4	49.7	44.2	0.112	0.233	−0.40	+0.10
80	59.1	56.0	47.4	0.089	0.163	−3.98	−2.50
85	64.7	65.7	48.9	0.056	0.092	−12.87	−15.90

Table 5.1. Selected results from the three runs (the 0.6 eV run used three seeds).

With E_a = 0.8 eV at 300 K an atom hops less than once before it is buried, and the film is indistinguishable from pure ballistic growth. With E_a = 0.6 eV each atom makes about 170–190 hops before burial. The film then fills in, roughly doubling its density, and the columns become shorter, rounder mounds (Figure 7). At glancing angles the measured tilt saturates near 45–49° instead of continuing to rise. At 80–85° the ridge spacing falls by a quarter to a half and the roughness by 15–25 %. The real value of E_a for SiO_2 on SiO_2, and the substrate temperature in the carousel, are therefore the most important unknowns for the film structure. Heating the substrate to 350 °C, as Lesker recommends for dense optical SiO_2, raises the hop rate by many orders of magnitude for a given E_a and pushes the film toward the 0.6 eV case.

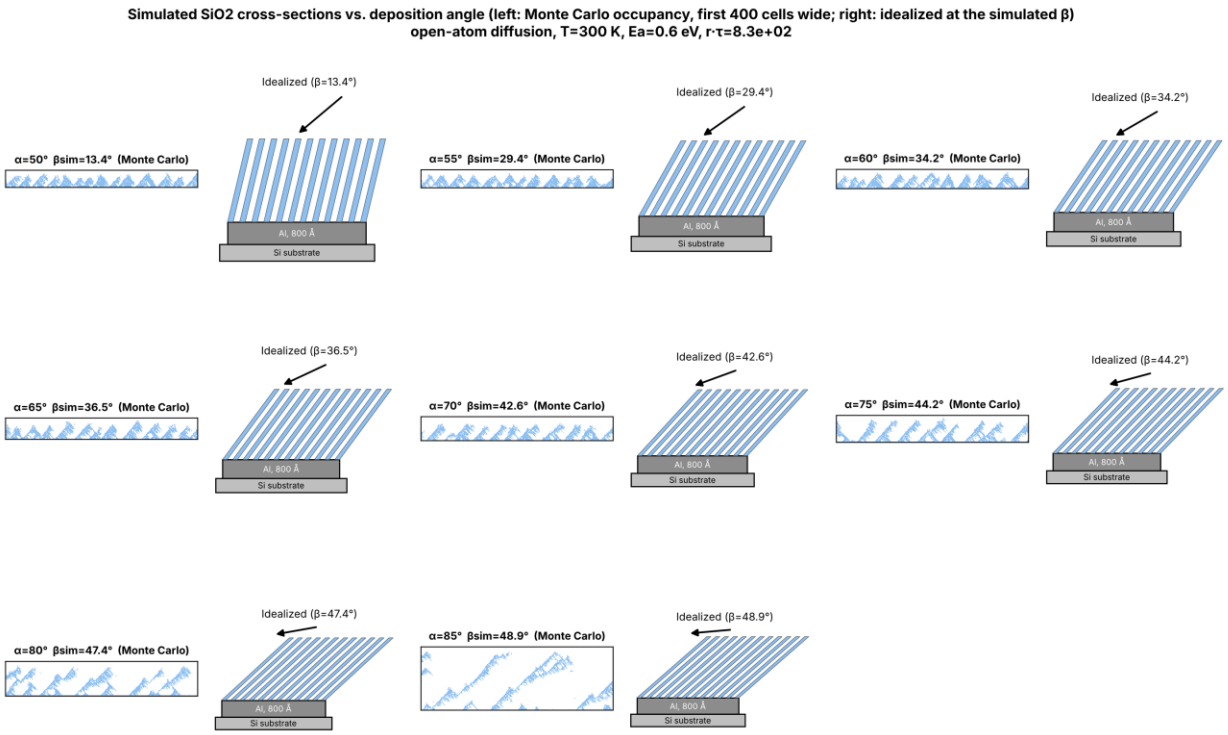


Figure 7. Simulated cross-sections with strong diffusion (E_a = 0.6 eV, 300 K): denser mounds and lower tilt at glancing angles.

6. Liquid-crystal pretilt

Model. Above the simulated surface, smoothed with a 4 nm Gaussian (a continuum nematic does not resolve sub-nanometer lattice steps), the director n = (sin θ, cos θ) in the plane of incidence minimizes

$$F = \iint \tfrac{1}{2}\,[K_1(\nabla\cdot\mathbf{n})^2 + K_3(\mathbf{n}\times\nabla\times\mathbf{n})^2]\,dx\,dz + \oint \tfrac{1}{2}\,W(s)\,\sin^2\!\big(\theta-\theta_e(s)\big)\,ds \qquad (6.1)$$

with Rapini–Papoular anchoring of strength W toward the local easy axis $\theta_e(s)$, here the local surface normal (homeotropic anchoring, as in a VA cell). The bulk term is linearized about the far-field tilt and solved by finite elements on a surface-fitted periodic mesh; the anchoring term is kept nonlinear. The pretilt is the average director tilt at the flat top of the mesh, 25 nm above the highest surface point. The weak-anchoring limit, the W-weighted average of the easy axes, is also reported.

Humidity. At relative humidity RH, water condenses by capillary action in valleys narrower than about twice the Kelvin radius

$$r_K = \frac{2\gamma V_m}{RT\ln(1/\mathrm{RH})} \qquad (6.2)$$

(1.5 nm at 50 % RH, 9.9 nm at 90 %), implemented as a rolling-disk closing of the surface. Adsorbed water also weakens the anchoring, $W = W_{dry}(1 - 0.5\,\mathrm{RH})$, and on water-filled regions the anchoring is 20 % of that. These humidity rules are phenomenological and need damp-heat data to calibrate.

α (°)	rms surface slope	Pretilt, dry (°)	Pretilt, 50 % RH (°)	Pretilt, 90 % RH (°)

α (°)	rms surface slope	Pretilt, dry (°)	Pretilt, 50 % RH (°)	Pretilt, 90 % RH (°)
50	0.32	+0.27 ± 0.28	+0.56	+0.77
60	0.37	+0.31 ± 0.08	+0.48	+0.66
70	0.44	+0.11 ± 0.24	+0.26	+0.10
75	0.55	−0.66 ± 0.35	−1.09	−1.57
80	0.72	−4.15 ± 0.98	−5.52	−6.79
85	0.93	−11.07 ± 1.44	−13.17	−14.99

Table 6.1. Predicted pretilt from the substrate normal for MLC-6608 (K_1 = 16.7 pN, K_3 = 18.1 pN), W_{dry} = 3 × 10^{-4} J/m^2 (extrapolation length 58 nm), E_a = 0.8 eV run. Positive = tilted toward the vapor source.

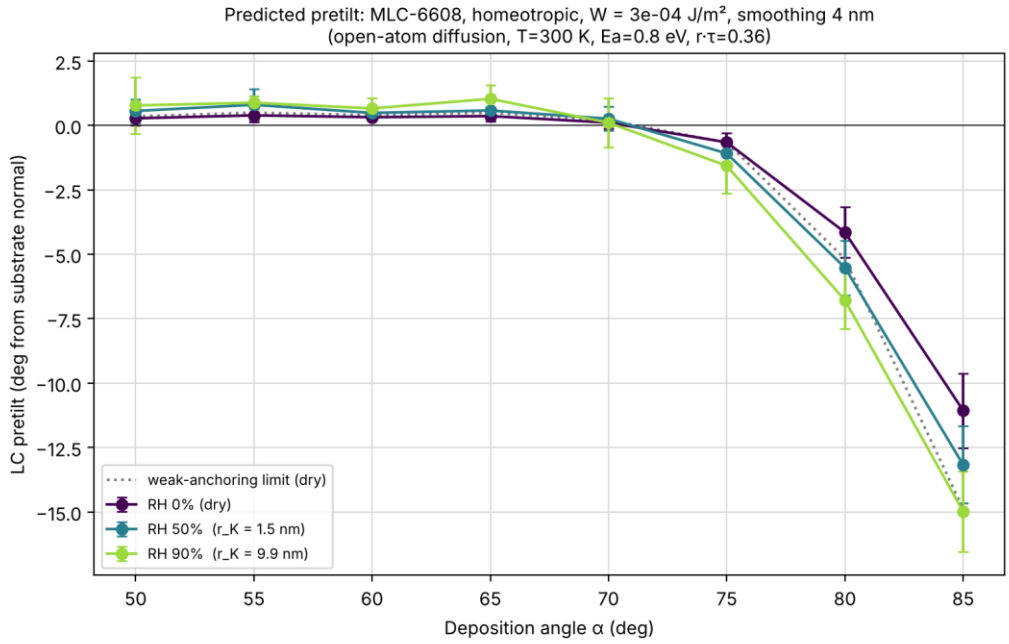


Figure 8. Predicted pretilt against deposition angle at 0, 50 and 90 % RH, with the dry weak-anchoring limit.

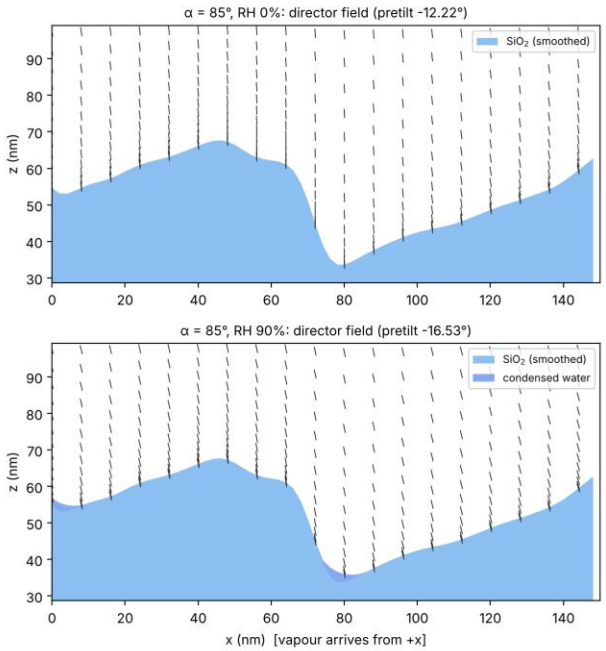


Figure 9. Director field above 150 nm of the α = 85° surface, dry (top) and at 90 % RH with condensed water (bottom).

A pretilt appears only when the distribution of surface slopes is asymmetric; a symmetric surface gives zero pretilt however rough it is. Up to about 70° the surface is nearly symmetric at the 4 nm smoothing scale and the pretilt is a fraction of a degree. Above 75° the long, gently sloping faces that look toward the source dominate the surface area. The director follows their normals, which lean away from the source, so the pretilt becomes negative and grows quickly with angle. Because the extrapolation length (58 nm) is much longer than the ridge height, the pretilt is close to the weak-anchoring limit (Figure 8), meaning it is set mainly by the area-weighted surface slope and only weakly by W.

Humidity increases the pretilt magnitude by about 1.5–4° at 80–85°. Water fills the narrow valleys at the foot of the steep shadowed faces (Figure 9), removing some of the slopes that oppose the dominant tilt, and the weaker anchoring lets the remaining slopes dominate further. If the real film behaves this way, the pretilt of a sealed cell would drift with the moisture absorbed during assembly and damp-heat aging.

7. Implications for the LCoS process

1. **Operating point in the SpatiaLight carousel.** The e-beam note puts the vapor incidence at 82.2° at the wafer center (81.0° at the bottom edge, 83.2° at the top). Interpolating Table 6.1 linearly, the predicted dry pretilt is about 5.5° at the bottom of the wafer, 7.2° at the center and 8.6° at the top. That range brackets the 8° used in the VAN cell model; the cell model shows that a smaller pretilt improves contrast and a larger one lowers the threshold slope, so the wafer-scale variation will appear as a threshold and contrast gradient.
2. **The column tilt is fixed early.** The tilt is constant after roughly the first 20 nm, so layer thickness can be chosen for durability and optical reasons (and for the material budget in the e-beam note) without changing the alignment.

3. **Substrate temperature matters.** If surface diffusion is active (low E_a or a heated substrate), the film is denser and its tilt and roughness at 80–85° are lower, which would reduce the pretilt at a given angle. A deposition-temperature series should be part of the first experiments.
4. **Packing fraction feeds the rate calculation.** The 2D model gives packing fractions of 0.06–0.17 without diffusion, far below the 0.5–0.7 typical of real columnar films, because a 2D cross-section exaggerates porosity. For the deposition-rate and thickness estimates in the e-beam note, a measured packing fraction (from ellipsometry or film-mass measurements) should be used rather than these values.
5. **Humidity control.** The predicted 1.5–4° pretilt shift with humidity argues for depositing, assembling and filling the cells in dry conditions and for a hermetic seal.

8. Calibration and measurement

Two parameters are calibration knobs rather than known quantities:

- **Smoothing length (4 nm).** Pure ballistic growth is much rougher than real films. With 1 nm smoothing the rms surface slope is about 1.5 and pretilts reach tens of degrees; with 4 nm the slope is 0.3–0.9 and pretilts are VA-like. The printed rms slope should be matched to AFM data, or the smoothing chosen so that one measured pretilt is reproduced.
- **Anchoring strength W.** The default 3×10^{-4} J/m^2 is a typical value for strong polar anchoring. Because the predicted pretilt lies close to the weak-anchoring limit, W mainly affects the humidity response.

Tkachenko, Marino and Abbate (2010), in this folder, describe how variable-angle spectroscopic ellipsometry measures the LC director distribution, pretilt and polar anchoring strength of filled cells, with and without applied voltage. That technique, applied to test cells made at two or three deposition angles, would fix both parameters and test the sign of the predicted tilt (whether the LC leans toward or away from the source), which the model cannot settle on its own. The `MEASURED_PRETILT` list in the script overlays such data on Figure 8.

9. Limitations

- **Two dimensions.** Growth is simulated in the plane of incidence only. Real GLAD columns also broaden and fan out sideways (out of this plane), which raises the density and changes the tilt; packing fractions here are therefore much lower than real.
- **Single sticking rule and one activation energy.** Particles stick on first contact and every hop costs the same E_a, whatever the site coordination.
- **SiO_2 chemistry.** The vapor is treated as SiO_2 units, although e-beam SiO_2 evaporates largely as $SiO + O_2$ and re-oxidizes on the surface.
- **Pretilt model.** It assumes a 2D director in the plane of incidence, a single anchoring strength and phenomenological humidity rules; azimuthal anchoring and twist are not included.
- **Thickness.** Films reach 27–77 nm in the default lattice, comparable to real alignment layers; a taller lattice (`NZ_LATTICE`) is needed to study thicker films.

References

1. J. M. Nieuwenhuizen and H. B. Haanstra, "Microfractography of thin films," *Philips Tech. Rev.* **27**, 87 (1966) (tangent rule).
2. R. N. Tait, T. Smy and M. J. Brett, "Modelling and characterization of columnar growth in evaporated films," *Thin Solid Films* **226**, 196 (1993).
3. A. Rapini and M. Papoular, "Distorsion d'une lamelle nématique sous champ magnétique conditions d'ancrage aux parois," *J. Phys. Colloq.* **30**, C4-54 (1969).
4. V. Tkachenko, A. Marino and G. Abbate, "Study of nematic liquid crystals by spectroscopic ellipsometry," *Mol. Cryst. Liq. Cryst.* **527**, 80 (2010) (copy in this folder).
5. Kurt J. Lesker Company, "Silicon Dioxide (SiO_2) Evaporation Process Notes" (copy in this folder).
6. B. S. McKeon, "Characterization of Silicon Dioxide Thin Film Deposition," B.S. thesis, Brigham Young University (2015) (copy in this folder).
7. S. Oh, "Nucleation and growth of nanostructures and films," lecture notes (copy in this folder).
8. Merck KGaA, MLC-6608 liquid-crystal data (K_1, K_3).
9. `OAD_SiO2_MonteCarlo_Simulation_8_xcorr_tilt.wl`, LCoS Simulations folder (original Mathematica model).